Hindawi
Complexity
Volume 2018, Article ID 6132139, 15 pages
https://doi.org/10.1155/2018/6132139

Research Article

GA-BPNN Based Hybrid Steering Control Approach for Unmanned Driving Electric Vehicle with In-Wheel Motors

Yong Li[1], **Xing Xu**[1] and **Wujie Wang**[2]

[1]*Automotive Engineering Research Institute, Jiangsu University, Zhenjiang 212013, China*
[2]*School of Automotive and Traffic Engineering, Jiangsu University, Zhenjiang 212013, China*

Correspondence should be addressed to Xing Xu; xuxing@mail.ujs.edu.cn

Received 12 July 2018; Accepted 28 August 2018; Published 13 November 2018

Academic Editor: Liang Hu

The steering system is a key component of the unmanned driving electric vehicle with in-wheel motors (IWM-EV), which is closely related to the operating safety of the vehicle. To characterize the complex nonlinear structure of the steering system of unmanned driving IWM-EV, a hierarchical modeling and hybrid steering control approach are presented. Firstly the 2-DOF model is introduced for the entire vehicle system, and then the models of the steering system and the in-wheel drive system are analyzed sequentially. The steering torque control system based on electronic differential (ED) and differential assist steering (DAS) is studied. The back propagation neural network (BPNN) is used to optimize the network structure, parameters, and the weight coefficient of the hybrid steering system. The genetic algorithm (GA) is employed to optimize the initial weight of BPNN and search within a large range. The GA-BPNN model is established with the yaw moment and differential torque as the input of BPNN. Simulation and experimental results show that the proposed GA-BPNN-based hybrid steering control approach not only accelerates the convergence speed of steering torque weight adjustment but also improves the response speed and flexibility of the steering system. Through optimizing and distributing the steering torque dynamically, the proposed GA-BPNN-based control approach has inherited the advantages of both vehicle stability under ED and the steering assistance under DAS, which further guarantees the safety and stability of unmanned driving IWM-EV.

1. Introduction

Unmanned driving technology not only improves the driving safety but also provides an effective way to solve traffic jam. After decades of research, unmanned driving is gradually evolving from semiautonomous to fully autonomous [1–3]. In-wheel motor drive electric vehicle is a kind of new energy vehicle with the drive motor installed inside the wheel. It has many advantages such as independently controllable drive torque, fast and accurate torque response, compact structure, and high energy efficiency [4–6]. Compared with traditional vehicle, an unmanned driving electric vehicle with in-wheel motors (IWM-EV) has significant advantages in safety, stability, and economy. It can improve vehicle safety, trajectory tracking, and flexibility. Therefore, the unmanned driving IWM-EV will be the main development direction of EV in the future.

The vehicle steering system is an important part of the IWM-EV, which is related to the operating safety of the whole vehicle. Currently, there are very few studies on the steering system of unmanned driving IWM-EV; however, the research on steering control of wheel motor drive vehicle provides a reference for the research on steering system of unmanned driving IWM-EV [7–12]. There are two main steering control approaches: the electronic differential (ED) control and the differential assist steering (DAS).

The electronic differential (ED) control strategy is introduced into the vehicle control system, which takes the speed and turning angle required by the unmanned driving vehicle as input and the speed of the two rear-drive motors as the output. The results show the function of the mechanical differential can be completely realized by ED controller [13]. The ED control system of in-wheel motor drive vehicle based on neural network and PID is constructed. By coordinating

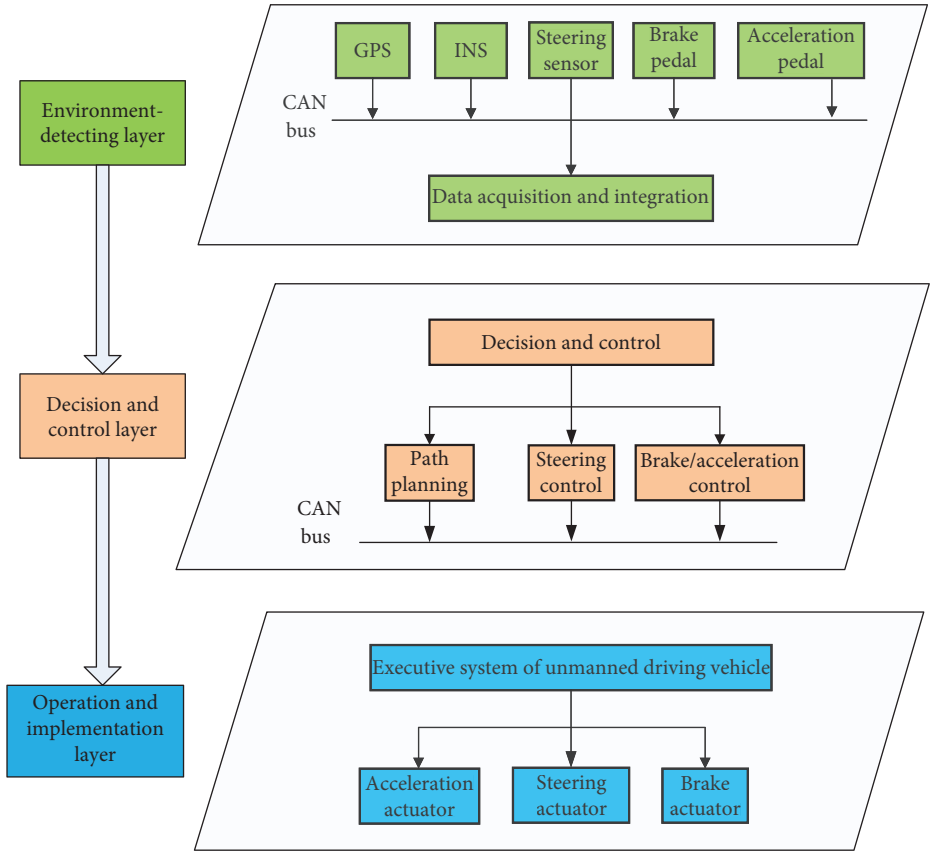

Figure 1: The configuration of the unmanned driving vehicle.

the torque of four in-wheel motors, the ED control steering is realized and the handling and stability of the low-speed steering of the vehicle are improved [14]. The vehicle yaw rate response and the handling performance of the vehicle are obviously improved through DAS control strategy, which reduces the steering wheel torque under the premise of ensuring the driver's road feeling [15]. The DAS control system is modeled and the wheel torque distribution control strategy is studied [16]. The DAS control strategy not only improves the vehicle driving stability but also satisfies the steering handiness.

However, single ED or DAS control cannot meet the differential and assist performance requirements of the in-wheel motor drive electric vehicle at the same time, especially in the case of turning operation, when the vehicle differential system is coupled with the assist steering system. Though theoretically both the ED control and the steering wheel assist control are needed to carry out by the difference of the in-wheel motor driving force, one single actuator cannot achieve two different dynamic control targets. Therefore, it is necessary to design a hybrid steering control strategy to coordinate the ED and DAS control.

On the other hand, the steering system of unmanned driving IWM-EV has exhibit characteristics of the complex structure, nonlinearity, time-varying, and multiparameters [17–19]. In addition, as a complex system of different components involving many disciplines such as mechanics, control, and information, the steering system is closely related to the vehicle operating safety. As a result, it motivates our in-depth investigation of the steering system.

This paper contributes a novel hybrid steering control strategy based on GA-BPNN for unmanned driving IWM-EV. The weight of ED control and DAS control is dynamically adjusted, and the steering torque is optimized and distributed through the proposed GA-BPNN approach. The hybrid control of ED and DAS for the steering system is achieved. The proposed GA-BPNN method not only improves the response speed and flexibility of the steering system but also guarantees the operating safety of the unmanned driving IWM-EV.

The paper is organized as follows. The configuration and modeling of unmanned driving IWM-EV are analyzed in Section 2. Section 3 presents the hybrid steering control approach based on GA-BPNN. The torque controller of the steering system is discussed in Section 4. In Section 5, the DAS, ED, and hybrid steering control approach are simulated. Section 6 is devoted to the road testing verification of DAS, ED, and GA-BPNN-based hybrid steering control approach. The conclusions of the work are presented in Section 7.

2. Configuration and Modeling of Unmanned Driving IWM-EV

2.1. Structure and Configuration. The configuration of unmanned driving IWM-EV studied in this paper is shown in Figure 1.

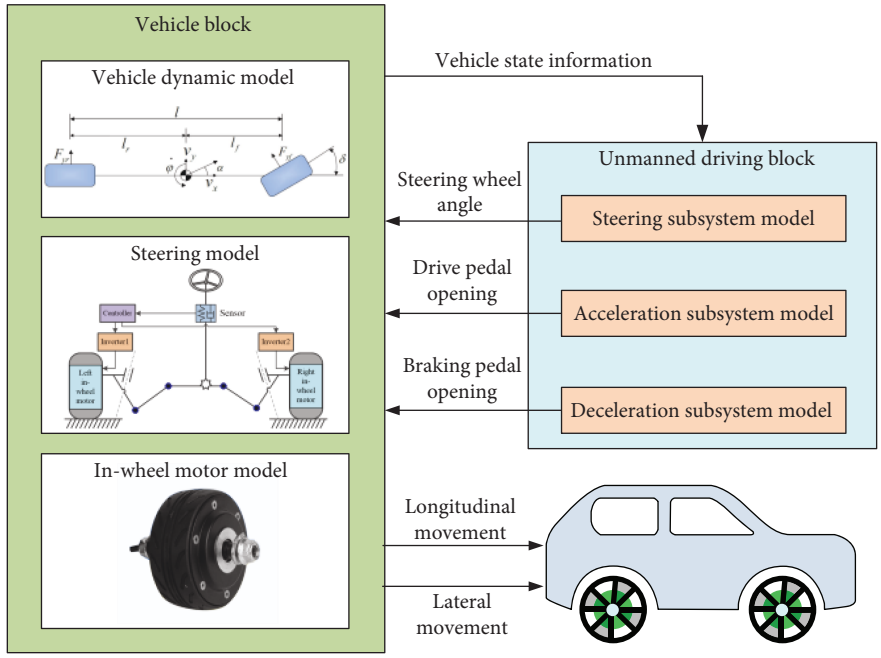

Figure 2: The dynamic model diagram of unmanned driving IWM-EV.

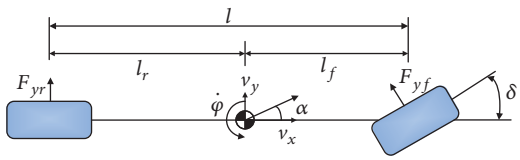

Figure 3: The linear model of 2-DOF unmanned driving IWM-EV.

It can be seen from Figure 1 that the unmanned driving IWM-EV is mainly composed of the environment-detecting module, the decision, control module, and the execution module. The environment-detecting module is the core control part of the unmanned driving vehicle, in which the GPS, INS, and sensor information should be analyzed and calculated. The operating performance of unmanned driving IWM-EV mainly determines on the computing ability of the environment-detecting module. GPS and INS are used to calculate the driving position, vehicle speed, and other information of the unmanned driving vehicle. The navigation parameters are analyzed to guide the unmanned driving IWM-EV to operate along the selected route accurately and safely [20–23].

Accurate and effective vehicle model provides a solid foundation for simulation and control. The dynamic model diagram of the unmanned driving vehicle is shown in Figure 2. The steering system of an unmanned driving electric vehicle with in-wheel motors has strong nonlinear property, which makes the intelligent vehicle has complex dynamic response [24, 25]. According to the vehicle dynamics of the vehicle in real operation, block modelling method is employed to reflect the vehicle motion condition, dynamical coupling, and nonlinear steering mechanism.

2.2. 2-DOF Model of Unmanned Driving IWM-EV. The dynamical steering process is complex with time variables. Two wheels on the front and rear axle can be simplified into one wheel. To analyze the unmanned driving vehicle with in-wheel motors, 2-DOF model of unmanned driving IWM-EV is established [26–28]. The linear reference model of 2-DOF is shown in Figure 3. F_{yf} and F_{yr} are the lateral force of tire, respectively.

$$\begin{bmatrix} \dot{v}_y \\ \ddot{\varphi} \end{bmatrix} = \begin{bmatrix} -\dfrac{V_{\mathrm{r}} + V_{\mathrm{f}}}{m v_x} & \dfrac{V_{\mathrm{r}} l_{\mathrm{r}} - V_{\mathrm{f}} l_{\mathrm{f}}}{m v_x} - v_x \\ -\dfrac{l_{\mathrm{f}} V_{\mathrm{f}} + l_{\mathrm{r}} V_{\mathrm{r}}}{J_z v_x} & -\dfrac{l_{\mathrm{f}}^2 V_{\mathrm{f}} + l_{\mathrm{r}}^2 V_{\mathrm{r}}}{J_z v_x} \end{bmatrix} \begin{bmatrix} v_y \\ \dot{\varphi} \end{bmatrix} + \begin{bmatrix} \dfrac{V_{\mathrm{f}}}{m} \\ \dfrac{l_{\mathrm{f}} V_{\mathrm{f}}}{J_z} \end{bmatrix} \delta, \tag{1}$$

where m is the vehicle mass. α is the slip angle of the vehicle. V_{f} and V_{r} are the cornering stiffness of front and rear tires, respectively. v_x and v_y are the longitudinal and lateral speed of the vehicle, respectively. $\dot{\varphi}$ is the vehicle yaw rate. l_{f} and l_{r} are the distance from the mass center to the front and rear wheel, respectively. J_z is the moment inertia of the vehicle around z-axis. δ is the steering angle of the front wheel.

The lateral control model can be expressed as

$$\begin{cases} \dot{X} = AX + BU + g(X, U) \\ Y = AX \end{cases}, \tag{2}$$

where $X = (v_y, \dot{\varphi}, y_{\mathrm{L}}, \varepsilon_L)^T$, y_{L} is the lateral deviation, ε_L is the azimuth deviation. $Y = (y_{\mathrm{L}}, \varepsilon_L)^T$. $u = (\delta)$. $g = (X, U)$ is the disturbance caused by unmodelled dynamics.

$$A = \begin{bmatrix} -\dfrac{V_r + V_f}{mv_x} & \dfrac{V_r l_r + V_f l_f}{mv_x} - v_x & 0 & 0 \\ -\dfrac{l_f V_f + l_r V_r}{J_z v_x} & -\dfrac{l_f^2 V_f + l_r^2 V_r}{J_z v_x} & 0 & 0 \\ -1 & -D_L & 0 & v_x \\ 0 & -1 & 0 & 0 \end{bmatrix}. \quad (3)$$

D_L is the preview distance.

$$B = \begin{bmatrix} \dfrac{V_f}{m} \\ \dfrac{l_f V_f}{J_z} \\ 0 \\ 0 \end{bmatrix}, \quad C = \begin{bmatrix} 0 & 0 & 1 & 0 \\ 0 & 0 & 0 & 1 \end{bmatrix}. \quad (4)$$

2.3. Steering Model. The steering system performance plays an essential role in the lateral stability control for an unmanned driving vehicle with in-wheel motors [25, 29–31]. To clearly describe the steering wheel and the steering system, the equivalent model of the steering system is established and shown in Figure 4.

Assuming the yaw rate is $\dot{\varphi}$ when the vehicle is turning round, the equivalent dynamic equations of the steering wheel and front wheel are described as

$$\begin{aligned} J_1\left(\frac{d^2\theta_1}{dt^2} + \frac{d\dot{\varphi}}{dt}\right) + C_1\frac{d\theta_1}{dt} + K_s(\theta_1 - \theta_2) &= T_1, \\ J_2\left(\frac{d^2\theta_2}{dt^2} + \frac{d\dot{\varphi}}{dt}\right) + C_2\frac{d\theta_1}{dt} - K_s(\theta_1 - \theta_2) &= T_2, \end{aligned} \quad (5)$$

where J_1 is the equivalent moment of inertia of the steering wheel. J_2 is the equivalent moment of inertia of the tire. θ_1 is the steering angle of the steering wheel round the pin. θ_2 is the steering angle of the tire. C_1 and C_2 are the equivalent damping coefficient of steering wheel around the pin, and the equivalent damping coefficient of output shaft of steering system, respectively. K_s is the torsional stiffness coefficient. T_1 is the torque of the steering wheel. T_2 is the torque on the tire caused by the tire cornering force around the kingpin.

2.4. In-Wheel Motor Model. The dynamic response of the in-wheel motor model can be simplified as a 2-order system [32–34]. The transfer function can be expressed as

$$G(s) = \frac{1}{2\zeta^2 s^2 + 2\zeta s + 1}, \quad (6)$$

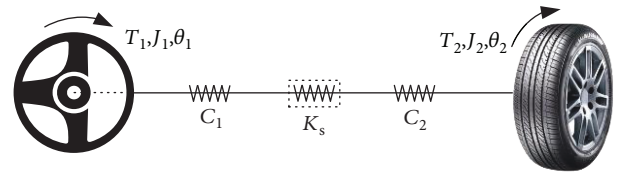

Figure 4: Equivalent model of the steering system.

where ζ is the coefficient determined by the in-wheel motor parameters.

The drive torque of the in-wheel motor is

$$T = p\left(\psi_d i_q - \psi_q i_d\right), \quad (7)$$

where p is the pole pair number of the in-wheel motor. ψ_d and ψ_q are the flux of the d-axis and q-axis. i_d and i_q is the flux of the d-axis and q-axis.

3. GA-BPNN-Based Hybrid Steering Control Approach

3.1. Hybrid Steering Control Scheme. To achieve the above-mentioned control purpose, the hybrid control approach is proposed as shown in Figure 5.

The hybrid control scheme consists of yaw-based electronic differential (ED) control, steering torque-based differential assist steering (DAS) control, and hybrid steering control based on GA-BPNN approach. ED and DAS constitute the upper layer controller, which is used to calculate the yaw rate torque for ED and differential torque according to the feedback vehicle speed, steering wheel torque, and angle signals from the vehicle dynamic model. The hybrid steering torque controller based on GA-BPNN in the lower layer is employed to dynamically adjust the weight of yaw rate torque and differential torque. The drive torque of the in-wheel motor in the left and right side are obtained finally. The weight is mainly determined by the vehicle speed. The weight of ED can be set for a large value to guarantee the vehicle stability in the high-speed range. The weight of DAS can be set for a large value to decrease the steering load in the low-speed range.

3.2. Back Propagation Neural Network. The 3-layer back propagation neural network (BPNN) is adopted in this paper. Assuming M is the node number in the input layer, H is the node number in the hidden layer, and N is the node number in the output layer. The control variable of ED is u_1 and the control variable of DAS is u_2. There are two nodes in the input layer, one is connected with ED controller and the other is connected with the DAS controller. Assuming the input and output set (X_p, T_p), $p = 1, 2, \ldots, P$, where P is the number of training samples. X_p is the input vector of the p-th sample, $X_p = (x_{p_1}, \ldots, x_{p_M})$. T_p is the expected output vector of the p-th sample, $T_p = (t_{p_1}, \ldots, t_{p_N})$, N is the number of dimensions of the output vector. $O_p = (o_{p_1}, \ldots, o_{p_N})$ is the real output vector of the neural network [35–37].

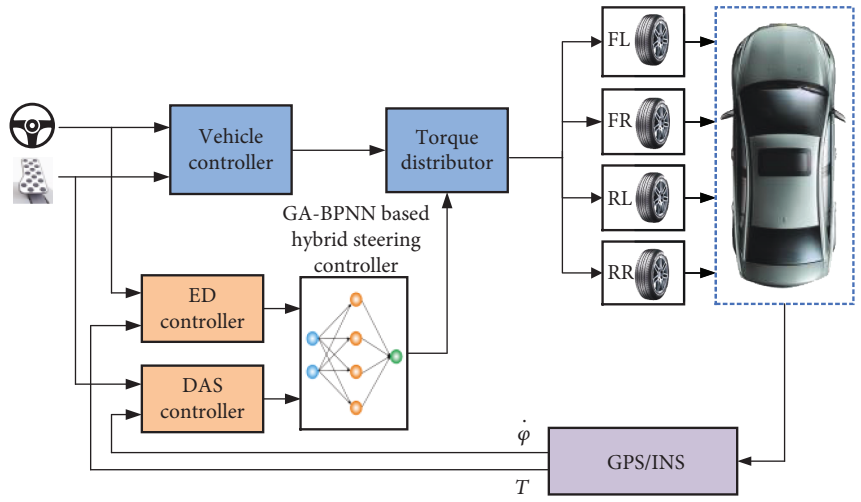

Figure 5: The principle of the coordinate control strategy.

The single hidden layer is employed in the BPNN. v_{ik} is the weight between the i-th node in the input layer and the k-th node in the hidden layer. w_{kj} is the weight between the k-th node in the hidden layer and the j-th node in the output layer.

Sigmoid described as (8) is the transfer function in the hidden and output layer.

$$f(x) = \frac{1}{1 + e^{-x}}. \tag{8}$$

The output of k-th node in the hidden layer is described as

$$y_{pk} = \eta_k f\left(\sum_{i=1}^{M} v_{ik} x_{pi}\right), \tag{9}$$

where y_{pk} is the output of k-th node in the hidden layer. x_{pi} is the input of i-th node in the input layer. $\eta_k \in [0, 1]$ is the impact factor of the k-th node in the hidden layer.

The output of j-th node in the output layer is expressed as

$$o_{pj} = f\left(\sum w_{kj} \eta_k f\left(\sum v_{ik} x_{pi}\right)\right). \tag{10}$$

Uniting (8), the differential of o_{pj} to η_k is

$$\frac{\partial o_{pj}}{\partial \eta_k} = \frac{o_{pj}(1 - o_{pj}) y_{pk} w_{kj}}{\eta_k}. \tag{11}$$

The impact factor change of η_k is shown as

$$\triangle \eta_k = \frac{\lambda \sum_{p=1}^{P} \sum_{j=1}^{N} (t_{pj} - o_{pj}) o_{pj} (1 - o_{pj}) y_{pk} w_{kj}}{\eta_k}. \tag{12}$$

The estimated value of j-th node in the output layer is expressed as

$$o_{pj}^{*} = f\left(\sum_{k=1}^{H} (w_{kj} + \triangle w_{kj}) y_{pk}\right). \tag{13}$$

where $\triangle \omega_{kj}$ is the weight change.

Combining (8) with (13), the weight change can be described as

$$\triangle w_{kj} = \frac{\sum_{p=1}^{P} \varphi_{pj} \cdot y_{pk}}{\sum_{p=1}^{P} \left(y_{pk}\right)^2}. \tag{14}$$

The sum of squares for error E can be obtained through $\triangle \omega_{kj}$. Then, an optimized value of k-th node in the hidden layer can be selected to get a minimum value for E.

3.3. Genetic Algorithm. Genetic algorithm (GA) is a new global optimization search method based on Darwin's theory of evolution and Mendel's genetic theory. The algorithm with strong robustness is suitable for parallel processing. It is widely used in computer science, optimization scheduling, transportation problems, combinatorial optimization, and other fields [38–40].

The GA can be described as

$$GA = (O(0), W, L, s, g, p, f, t), \tag{15}$$

where $O(0) = (a_1(0), a_2(0), \ldots, a_W(0)) \in I^W$ is the initial population? $I = \{0, 1\}$ is the set of a binary string of L. W is chromosome number in the population. L is the length of the binary string. $s : I^W \to I^W$ is the selection strategy. g is the genetic operator, including the reproduction operation $Qr : I \to I$, hybridization operation $Qc : I \times I \to I \times I$, and mutation operation $Q_m : I \to I$. p is the operation probability, including reproduction probability p_r, hybridization

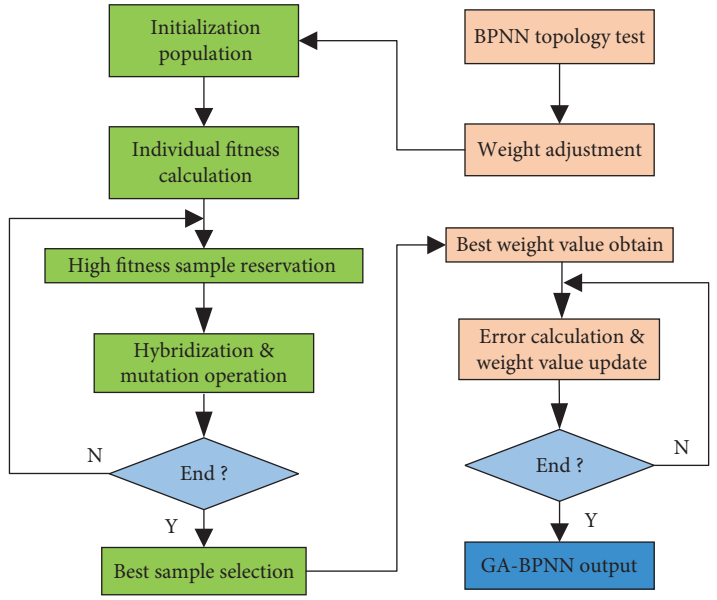

Figure 6: The flow chart of the proposed GA-BPNN.

probability p_c, and mutation probability p_m. $f : I \to R^+$ is the fitness function. $t : I^W \to \{0, 1\}$ is the stop criterion.

3.4. GA-BPNN Based Hybrid Control. The BPNN and GA are hybridized as GA-BPNN to optimize the initial weight. The weight and threshold value will be updated by heredity and mutation to minimize the total square error of GA-BPNN [41–43]. The flow chart of the proposed GA-BPNN is illustrated in Figure 6.

The procedures of GA-BPNN are shown as follows:

(1) The initial population $X(t) = \{x_1(t), x_2(t), \ldots, x_W(t)\}$ is generated randomly. The fitness values of all samples $x_i(t) \in X(t)$ are also calculated. The new population $X'(t)$ will be generated by hybridization operation and mutation operation with hybridization probability p_c andp_m, respectively

(2) Calculating the fitness of each sample in $X'(t)$. The next generation population $X(t+1)$ will be obtained by the optimization strategy

(3) The training will not end until the output training error of the optimized sample in the newly generated population is less than 10^{-3}. Otherwise, the evolution continues

The GA is employed to train the BPNN. The fitness function of GA is expressed as

$$F = \left[\frac{1}{2}\sum_{i=1}^{s_t}\left[y'(i) - y(i)\right]^2\right]^{-1}, \tag{16}$$

where $y'(i)$ is the output of i-th input sample. $y(i)$ is the expected output. S_t is the total learning sample number.

The error of the selected high-quality sample is guaranteed to be small through (16).

4. Torque Controller of Steering System

4.1. DAS Controller. The wheel dynamic can be described as

$$T = Fr_w + J_\omega \frac{d\omega}{dt}, \tag{17}$$

where F is the vertical drive force of the tire. r_w is the radius of the wheel. J_ω is the moment inertia of the wheel. ω is the angular speed of the wheel.

Assuming the drive torque of the in-wheel motors in the left and right side are T_l and T_r, respectively. The longitudinal drive force of the tire are F_l and F_r, respectively. T_{sl} and T_{sr} are the torque around the left and right drive wheels, which can be expressed as

$$\begin{aligned} T_{sl} &= F_l \cdot r_\sigma, \\ T_{sr} &= F_r \cdot r_\sigma, \end{aligned} \tag{18}$$

where r_σ is the scrub radius.

T_{sl} is equal to T_{sr} in the traditional mechanical steering system. However, drive torque difference T_s is caused by the different drive force from the left and right in-wheel motors.

$$\begin{aligned} T_s &= T_{sl} - T_{sr} = (F_l - F_r) \cdot r_\sigma \\ &= \left[(T_l - T_r) - J_w\left(\frac{d\omega_l}{dt} - \frac{d\omega_r}{dt}\right)\right] \cdot \frac{r_\sigma}{r_w}. \end{aligned} \tag{19}$$

The drive torque difference is delivered to the pinion and rack system by the steering arm, which propels the steering tie rod to move. Therefore, the steering assistance is achieved

through the proper control of in-wheel motors in the left and right side [44].

4.2. Direct Yaw-Moment Controller. According to the 2-DOF vehicle model, the expected yaw rate can be expressed as

$$\dot{\varphi}_e = \frac{v\delta}{nv^2 + l}, \tag{20}$$

where $\dot{\varphi}_e$ is the expected yaw rate. v is the vehicle speed. n is the vehicle stability coefficient.

The response of $\dot{\varphi}$ to the front wheel angle δ can be described as

$$\frac{\dot{\varphi}(s)}{\delta(s)} = \frac{gv}{1 + uvs}, \tag{21}$$

where g and u are determined by the vehicle parameters, respectively.

The above formula on the slip model surface is expressed as

$$S = uv\ddot{\varphi} + \dot{\varphi} - gv\delta = 0. \tag{22}$$

Eq. (20) should satisfy the following condition

$$\dot{S} + zS = 0 (z > 0). \tag{23}$$

The yaw moment controlled can be obtained

$$T_{\dot{\gamma}} = \frac{-z\gamma + \mathrm{gv}\dot{\delta} + \mathrm{zgv}\delta}{\mathrm{uvs} + \mathrm{zus} + 1} J_z - F_{y1} l_f + F_{y2} l_r. \tag{24}$$

The yaw moment controller based on the slide mode control scheme can well track the expected value [45, 46].

5. Simulation Verification

5.1. Steering Torque Control

5.1.1. Differential Assist Steering Simulation. Steering handiness is the basic criterion for testing the effect of differential assistance. This section will carry out model simulation tests with different steering wheel input at low vehicle speeds. Simulation results with DAS control and without torque distribution are compared and analyzed. When the vehicle is operating at low speed, steering wheel angle ramp input model is simulated to emulate the low-speed and sharp-turn test of the vehicle. The steering wheel angle ramp input starts at 3 s. The steering wheel angle change rate is 180°/s. One second later, the steering wheel input keeps at a constant value 180°. The steering wheel torque and vehicle trajectory are compared in Figures 7 and 8, respectively.

It can be seen from Figure 7 that DAS control scheme effectively reduces the steering wheel torque and steering load at low speed, especially in the process of the steering wheel angle change. Figure 8 illustrates that the turning radius of the vehicle is smaller under DAS control due to the different drive torque of the left and right in-wheel motor

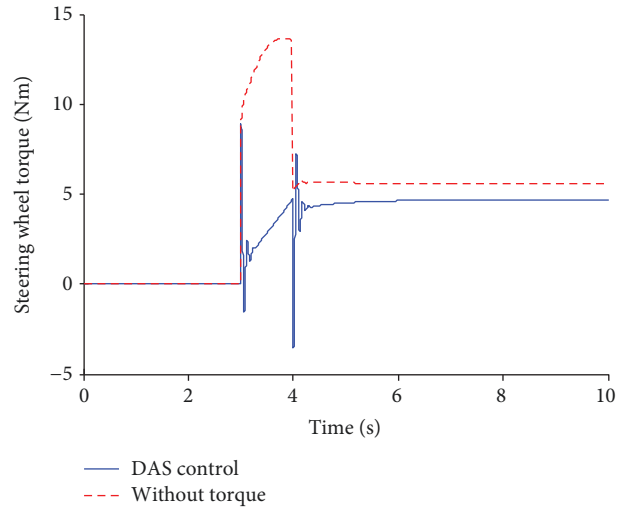

Figure 7: Comparison of steering wheel torque.

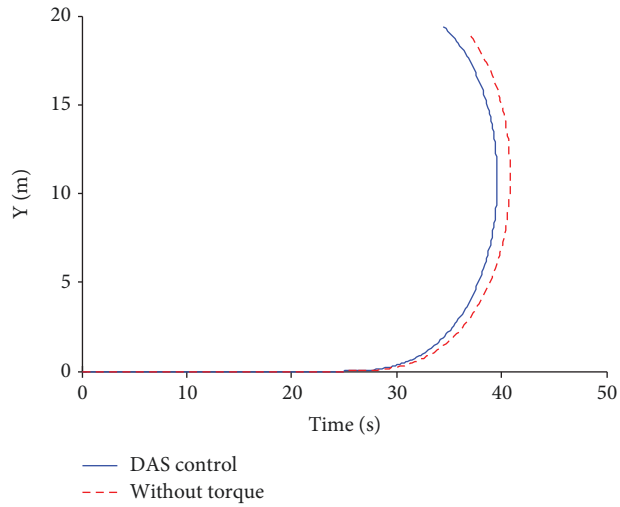

Figure 8: Comparison of vehicle trajectory.

under DAS control. The left and right in-wheel motor torque shown in Figure 9 generates an extra yaw moment to the vehicle, which finally reduces the under-steering performance of the vehicle and improves the cornering ability. The response curve in Figure 10 also illustrates the yaw rate is increased due to the extra yaw moment.

5.1.2. Electronic Differential Simulation. To verify the effectiveness of the sliding mode control for ED, the steering wheel angle step input and sine input are modeled and simulated. Simulation results under ED; the expected results in the ideal state and without distribution are compared and analyzed. The steering wheel angle step input is simulated to emulate the obstacle avoidance condition for a real-time vehicle, which is used to identify the ED performance and vehicle stability. The steering wheel angle is shown in Figure 11. The vehicle operates at a certain speed for 3 s. After that, the steering angle turns 30° to the left for 1 second and keeps the same angle.

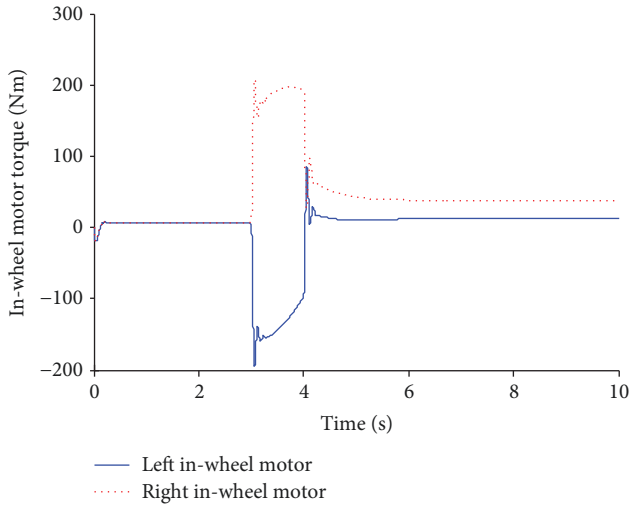

Figure 9: Left and right in-wheel motor torque.

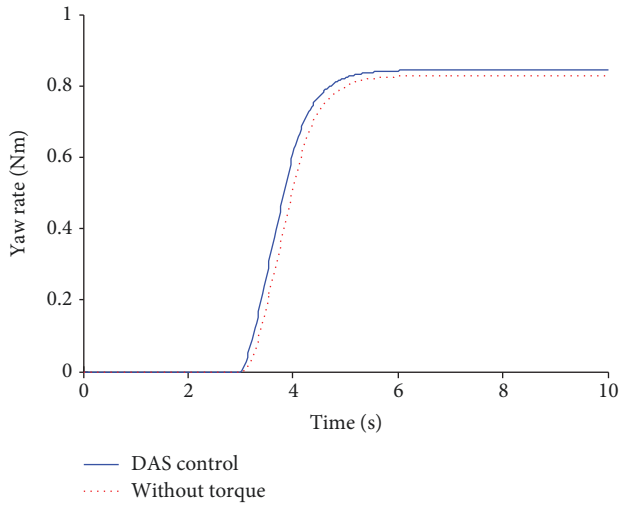

Figure 10: Comparison of vehicle yaw rate.

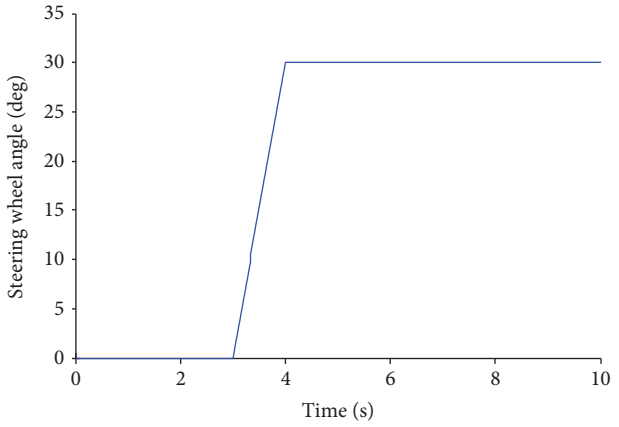

Figure 11: Steering wheel angle step input.

From the vehicle trajectory in Figure 12, it can be seen that the vehicle's turning radius under ED control is obviously smaller than that without ED control. The turning

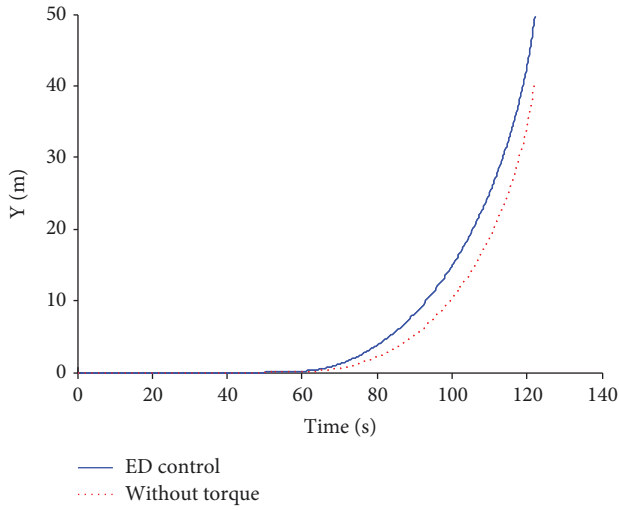

Figure 12: Comparison of vehicle trajectory.

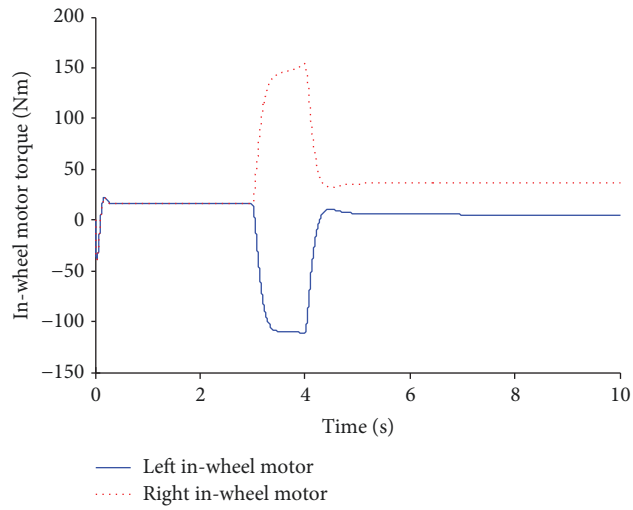

Figure 13: Left and right in-wheel motor torque.

performance of the vehicle is improved. This is mainly caused by the different drive torque of the left and right wheels, which are no longer the same under the ED control. Figure 13 shows the drive torque of the outer wheel is larger than that of the inner wheel, which means an extra yaw moment is added to the vehicle. Figure 14 shows the yaw rate curve of the vehicle under the step input of the steering wheel angle. It can be seen the vehicle yaw rate under ED control can better track the ideal yaw rate, even though there is a slight overshoot a small steady-state deviation. Both of the change response and the final steady-state value under ED control are larger than that under without torque distribution. This is also caused by the additional yaw moment.

5.2. Hybrid Steering Control. To verify the effectiveness of the weight generated by the proposed GA-BPNN, the simulation of steering wheel angle step input in variable speed is designed. The initial speed is set at 20 km/h. And it accelerates with 3 m/s^2 from the 5 s. The speed curve and steering

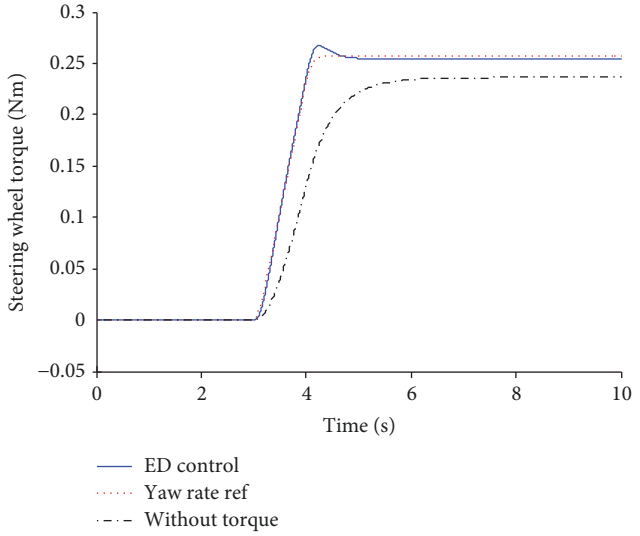

Figure 14: Comparison of vehicle yaw rate.

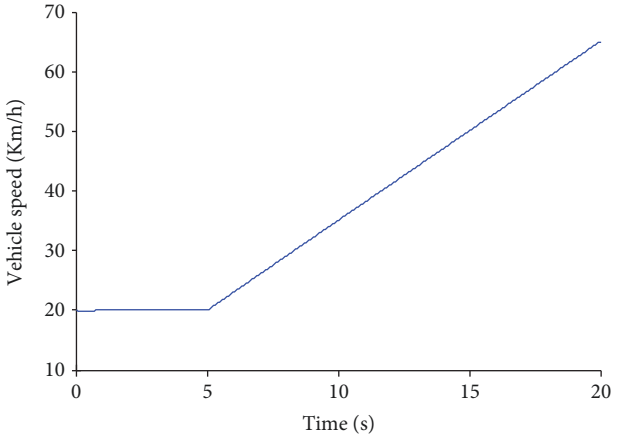

Figure 15: Vehicle speed of simulation.

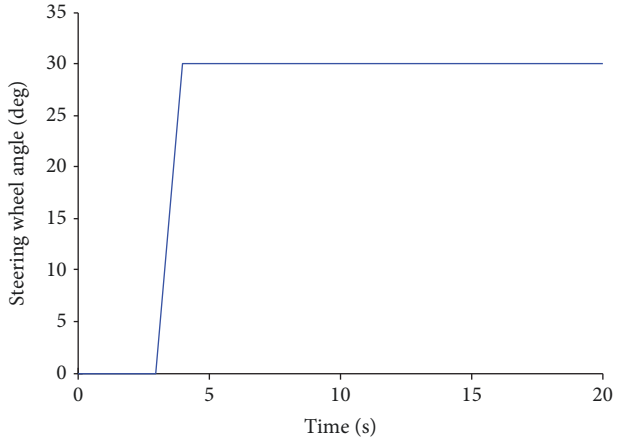

Figure 16: Steering wheel angle.

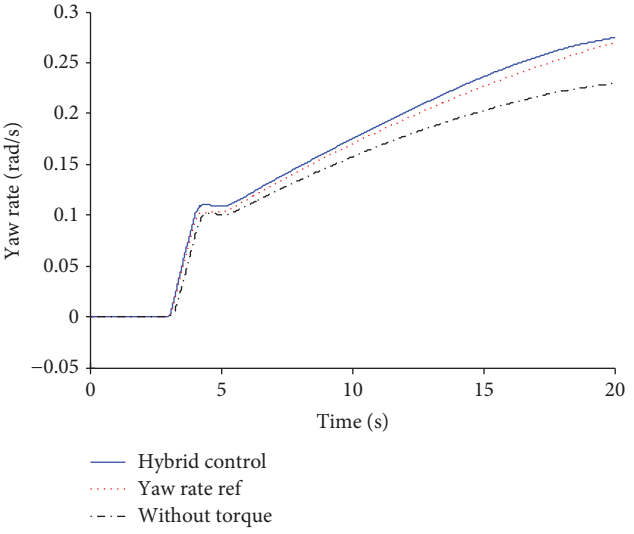

Figure 17: Comparison of vehicle yaw rate.

angle are shown in Figures 15 and 16, respectively. The simulation results of the vehicle rate of the proposed GA-BPNN-based hybrid steering control and without torque distribution are compared in Figure 17. It can be seen that the vehicle yaw rate without torque distribution is less than the ideal value, and the vehicle has severe understeer characteristics.

The yaw rate of the vehicle with GA-BPNN control approach is close to the ideal value. And the error increases first and then decreases. The main reason is the weight of ED is smaller than that of DAS at low speed shown in Figure 18. That leads to increasing error of the vehicle yaw rate. Figure 18 shows that the weight of ED goes up with the increasing vehicle speed, and the weight of DAS decreases. ED plays the major role in the hybrid steering control when the vehicle speed increases. That is why the yaw rate of the vehicle is smaller than the ideal value.

Figure 19 illustrates the steering wheel torque is effectively decreased due to the proposed GA-BPNN-based hybrid steering control scheme. And the steering wheel torque with hybrid steering control is close to the ideal value.

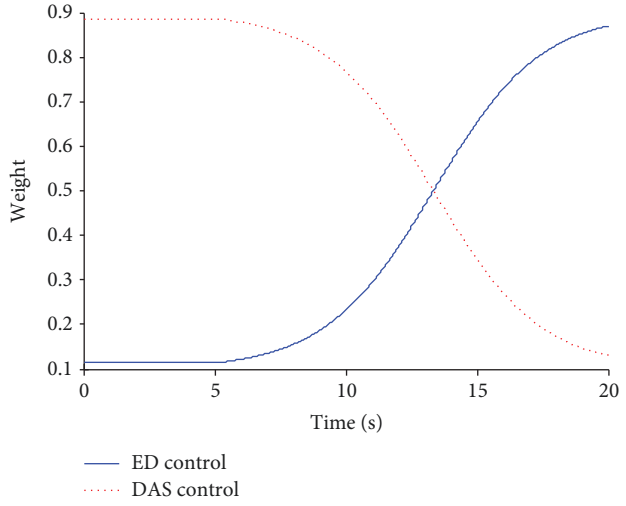

Figure 18: Weight coefficient.

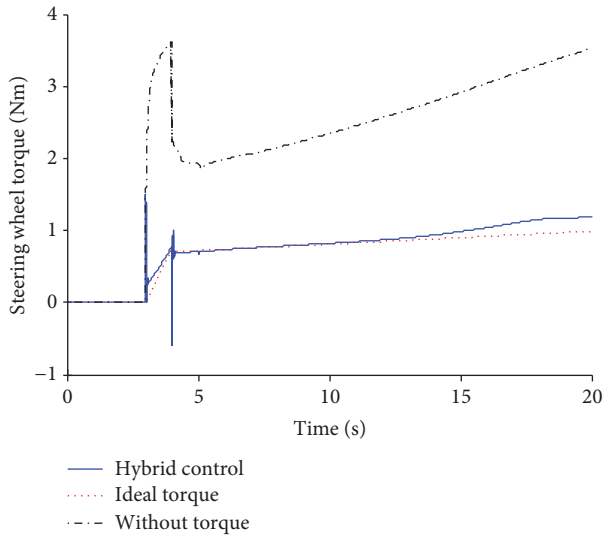

Figure 19: Comparison of steering wheel torque.

Figure 20: Test vehicle of UJS.

Also, it can be seen that the error between the steering wheel torque and the ideal value increases firstly and then keeps a constant value. This is caused by the major ED control in the hybrid steering process with the increasing vehicle speed.

6. Experimental Verification

To further verify the proposed GA-BPNN-based hybrid steering control approach, the experiment is carried out under snake testing. The test vehicle of UJS is shown in Figure 20. The vehicle parameters are shown in Table 1. The driver stays in the vehicle to guarantee the operating safety during the road testing. The D2P-Moto Hawk is used for designing the upper vehicle controller. And the signals from the controllers and sensors are measured, recorded, and passed by CAN bus.

The snake testing shown in Figure 21 is used to verify the proposed approach. The pile spacing in the snake testing is 30 m. The testing should be carried out on a sunny day without wind to guarantee the INS can receive the satellite signals accurately. The INS should be activated before the testing, during which the vehicle must operate on straight campus road. And, the test should be carried out on a smooth and well-paved cement yard. The road surface with a 0.85 road surface adhesion coefficient is used for the verification due to the limited test condition.

Table 1: Vehicle parameters.

Symbol	Parameter	Value
m	Vehicle mass	700 kg
L	Axle distance	1.77 m
L_f	Distance from the centroid to the front axle	0.795 m
L_r	Distance from the centroid to rear axle	0.975 m
J_z	Moment of inertia	2000 kg·m^2
r_w	Radius of wheel	0.245 m
V_f	Cornering stiffness of the front tire	30,000 N/rad
V_r	Cornering stiffness of the rear tire	30,000 N/rad
J_1	Moment of inertia of steering wheel	0.0015 kg/m^2
J_2	Moment of inertia on output shaft of steering system	0.0036 kg/m^2
C_1	Damping coefficient of steering wheel	0.27 N/(m·s)
C_2	Damping coefficient of output shaft of steering system	386.408 N/(m·s)
Ks	Torsional stiffness	41039.6 N/m

6.1. Steering Torque Control Road Testing

6.1.1. Differential Assist Steering. The weight of ED is set to be 0 and the weight of DAS is set to be 1 initially during the snake testing. Then, the steering wheel torque is used as the control target, the GA-BPNN hybrid steering controller will distribute the drive torque for the left and right in-wheel motors. The measured vehicle speed is shown in Figure 22. It can be seen that the speed of the vehicle basically keeps constant at 15 km/h after the 20s. The speed fluctuation at the 40s is mainly caused by the bumps on the test road.

Figure 23 shows the steering wheel angle and the torque curve. The fluctuations of the steering wheel angle and torque before the 20s are mainly caused by the adjustment of the vehicle driving direction during acceleration. The amplitude of the steering wheel angle keeps a constant value at around 50 degrees. Figure 24 shows the steering wheel torque changes with the steering steel angle. It can be seen the peak value of the steering wheel angle is about 50 degrees, and the peak value of the steering wheel torque is about 1 Nm under DAS control. Compared with Figure 7, it can be seen that the steering wheel torque is lower with DAS control shown in Figure 24. That is caused by the torque distribution of the left and right in-wheel motor under DAS control.

The control signals of the left and right in-wheel motors are shown in Figure 25. It can be seen that the driving force of the left and right in-wheel motors is redistributed by the GA-BPNN hybrid steering control scheme. Therefore, the abovementioned DAS effect is generated due to the driving

Figure 21: Overview of snake testing.

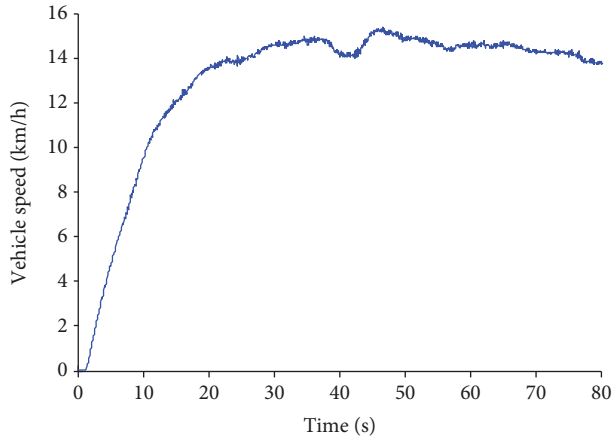

Figure 22: Vehicle speed of road test.

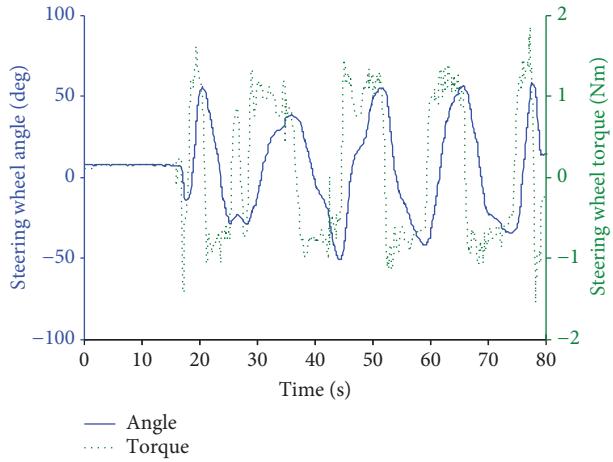

Figure 23: Steering wheel torque and angle.

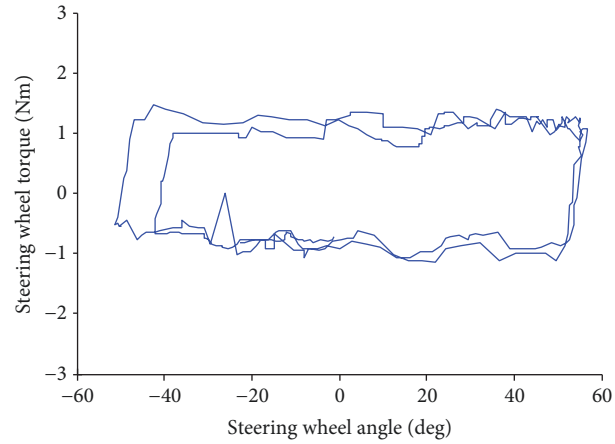

Figure 24: The relationship between steering wheel torque and angle.

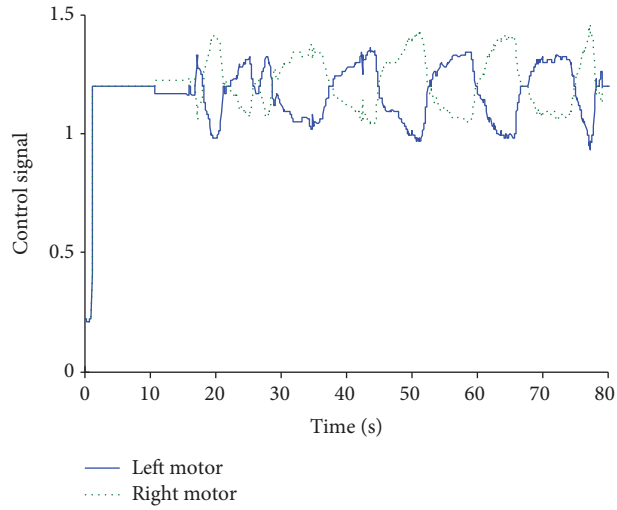

Figure 25: The control signal of in-wheel motors.

force of the outer in-wheel motor is greater than that of the inner in-wheel motor.

6.1.2. Electronic Differential Testing. The weight of ED is to be 1 and the weight of DAS is set to be 0 for the ED control. The vehicle yaw rate is used as the control target. The driving force of the left and right in-wheel motors is distributed by the GA-BPNN-based hybrid steering control scheme. Figure 26 illustrates the vehicle speed keeps a constant value at 15 km/h after the 20s. The speed fluctuation at 45 s is caused by the bumps on the test road.

Compared with Figure 7, it can be seen that the steering wheel torque is lower with ED control shown in Figure 27. That is caused by the torque distribution of the left and right in-wheel motor under ED control. An extra yaw moment is generated due to the different drive torque of the left and right in-wheel motors, which has some certain of steering assist effect.

Figure 28 shows the relationship between the steering wheel torque and the angle. It can be seen that the torque peak of the steering wheel is about 2 Nm when the steering wheel angle is about 50 degrees under ED control. Compared with the steering wheel torque angle of 15 km/h vehicle speed under without distribution control, it can be found that the steering wheel torque is reduced after the ED control. Figure 29 shows the control signals of the left and right in-wheel motors. It can be seen the proposed GA-BPNN based hybrid steering controller re-distributes the left and right in-wheel motor drive forces. The driving force of the outer

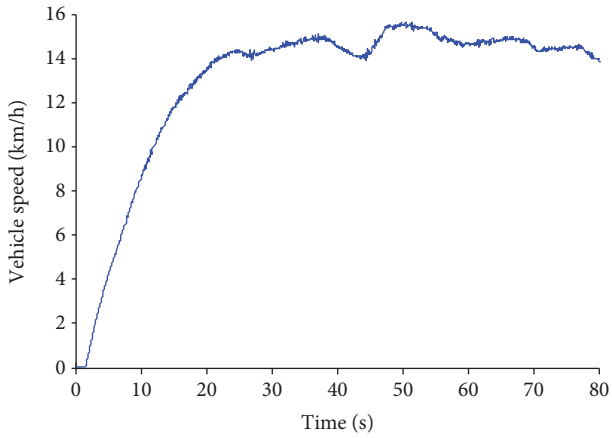

Figure 26: Vehicle speed of road test.

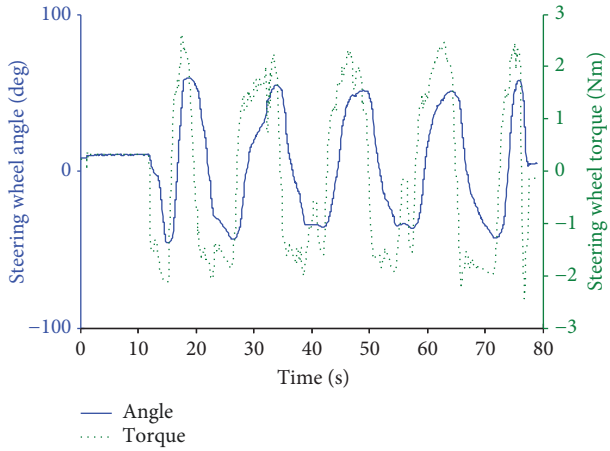

Figure 27: Steering wheel torque and angle.

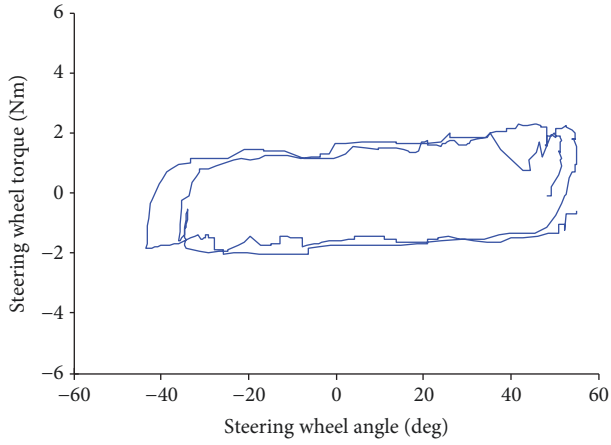

Figure 28: The relationship between steering wheel torque and angle.

in-wheel motor is greater than that of the inner in-wheel motor, which generates the above additional yaw moment.

6.2. Hybrid Control Road Testing. When the hybrid steering control is carried out for the snake testing, the weight of ED and DAS changes with the vehicle speed. The weight of yaw moment for ED control and the weight of differential torque for DAS control are adjusted by the proposed GA-BPNN hybrid steering controller according to the brake/acceleration pedal signal. The steering wheel torque and vehicle yaw rate are set as the control targets based on the current vehicle speed to redistribute the driving force of the left and right in-wheel motor. The vehicle speed is shown in Figure 30. It can be seen the vehicle speed keeps a constant value at about 15 km/h after the 20s. The speed fluctuation occurring at about 40s is also caused by the bumps on the test road.

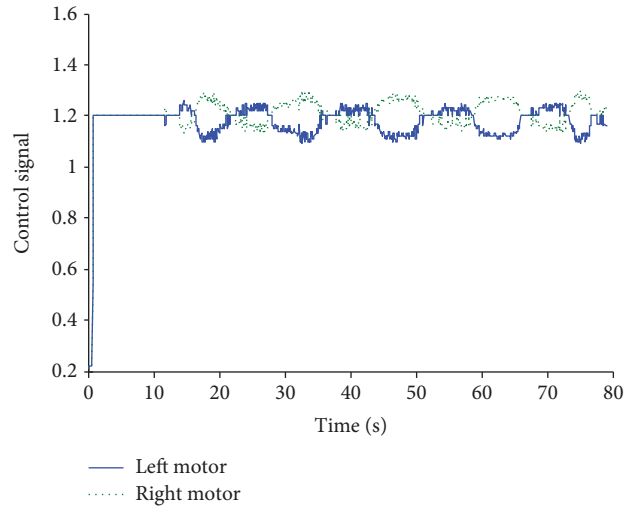

Figure 29: The control signal of in-wheel motors.

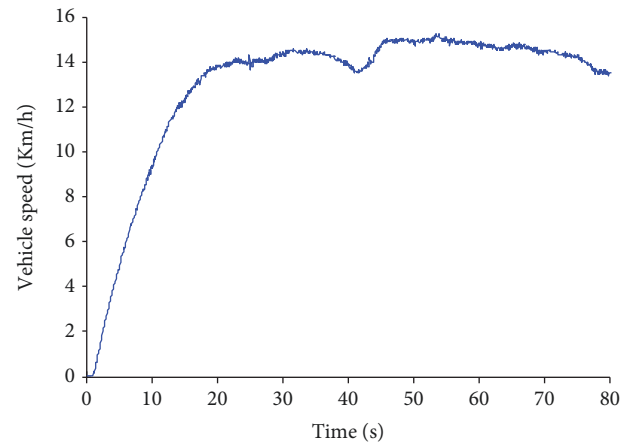

Figure 30: Vehicle speed of road test.

The steering wheel angle and the torque curve are shown in Figure 31. The steering wheel angle and torque fluctuations before the 20s are mainly caused by the adjustment of the vehicle operation direction during acceleration. The steering wheel angle keeps a constant value at 50 degrees. And the steering wheel torque changes with the steering wheel angle.

Figure 32 shows the relationship between steering wheel torque and rotation angle under the proposed GA-BPNN-based steering control. It can be seen that the peak torque of the steering wheel is about 1 Nm when the steering wheel angle is about 50 degrees. Compared with the steering wheel

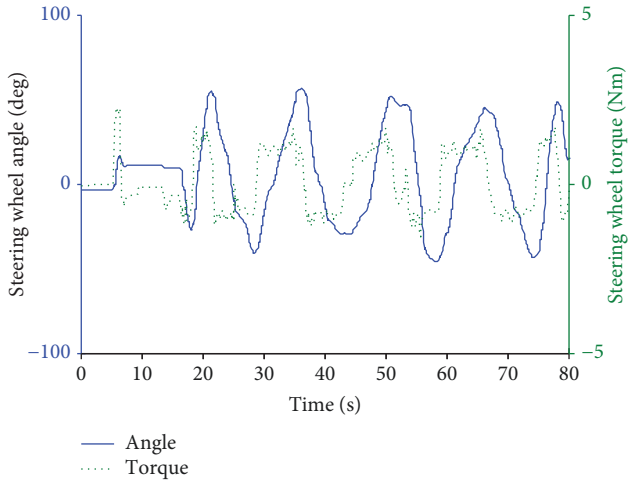

Figure 31: Steering wheel torque and angle.

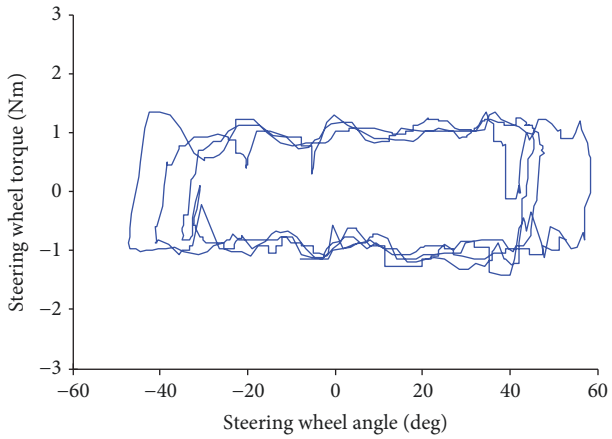

Figure 32: The relationship between steering wheel torque and angle.

torque angle of 15 km/h vehicle speed under without torque distribution control, it can be found that the steering wheel torque is significantly reduced after the differential control.

Figure 33 shows the control signals of the left and right in-wheel motors. It can be seen that the left and right in-wheel motor driving force are redistributed by the proposed GA-BPNN-based steering control approach. The abovementioned hybrid control effect is generated due to the driving force of the outer in-wheel motor is greater than that of the inner in-wheel motor.

Figure 34 illustrates the weight coefficient curves of ED and DAS in the hybrid steering control. The weight of ED control is adjusted to be 0.1 and weight of DAS control is adjusted to be 0.9 when the vehicle accelerates from 0 km/h to 15 km/h. Figure 35 shows the weight coefficient curves of ED and DAS in the hybrid steering control. The weight of ED control increases and weight of DAS control decreases when the vehicle accelerates from 0 km/h to 35 km/h. The effectiveness of the proposed GA-BPNN steering control approach is verified.

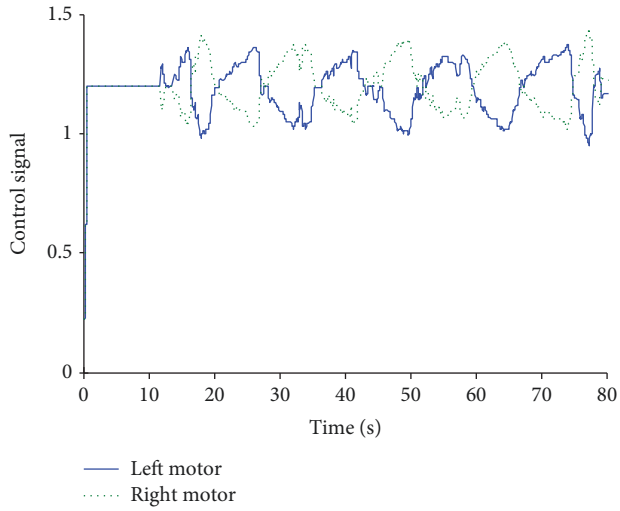

Figure 33: The control signal of in-wheel motors.

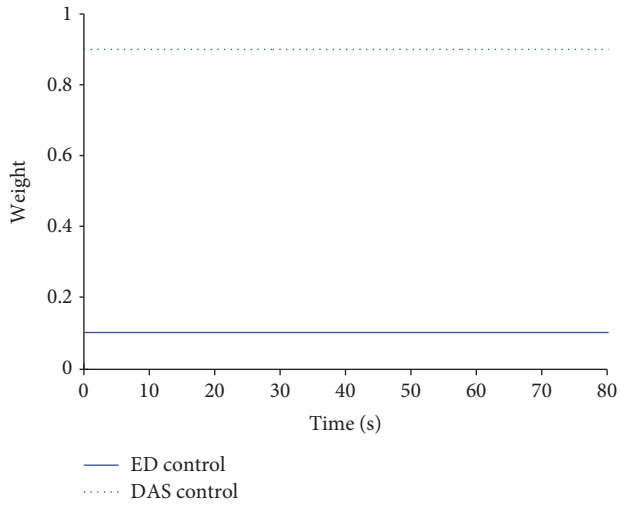

Figure 34: Weight coefficient.

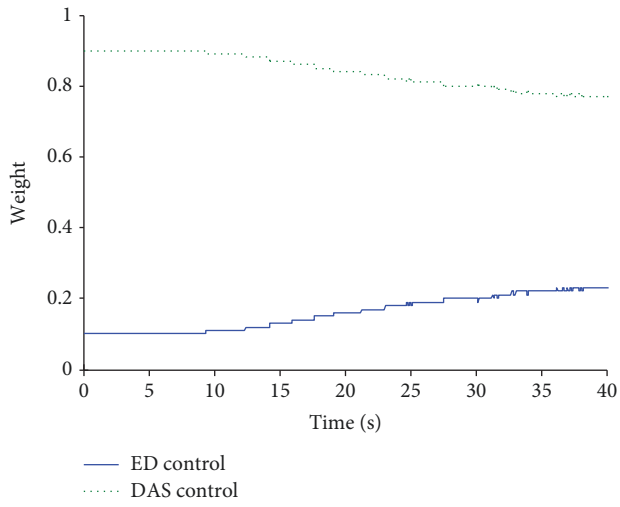

Figure 35: Weight coefficient.

7. Conclusion

Aiming at the complexity of the steering system of the unmanned driving IWM-EV, GA-BPNN-based hybrid steering control approach is proposed according to the analysis of the dynamic characteristics of the steering system. CarSim/MATLAB cosimulation and real vehicle test are carried out on the proposed GA-BPNN hybrid control strategy. Both of the simulation and experimental results show that the proposed hybrid steering control approach can not only satisfy the steering requirements of the unmanned driving vehicle but also accurately realize the steering function with fast response and stability performance. The GA-BPNN-based hybrid steering control approach proposed in this paper provides a solid foundation for the research on the stability of unmanned driving IWM-EV.

Data Availability

The data used to support the findings of this study are available from the corresponding author upon request.

Conflicts of Interest

The authors declare that they have no conflicts of interest.

Acknowledgments

This work was supported in part by the Primary Research & Development Plan of Jiangsu Province (BE2017129), the Open Research Subject of Key Laboratory of Vehicle Measurement, Control and Safety of Sichuan Province (SZJJ2017-076), Jiangsu Key Laboratory of Drives and Intelligent Control of Electric Vehicles (JLDICEV20150704), and the Initial Funding for Advanced Talents at Jiangsu University (15JDG164).

References

[1] A. Chamseddine, O. Akhrif, G. Charland-Arcand, F. Gagnon, and D. Couillard, "Communication relay for multiground units with unmanned aerial vehicle using only signal strength and angle of arrival," *IEEE Transactions on Control Systems Technology*, vol. 25, no. 1, pp. 286–293, 2017.

[2] P.-L. Blyth, M. N. Mladenovic, B. A. Nardi, H. R. Ekbia, and N. M. Su, "Expanding the design horizon for self-driving vehicles: distributing benefits and burdens," *IEEE Technology and Society Magazine*, vol. 35, no. 3, pp. 44–49, 2016.

[3] W. Wang and D. Zhao, "Extracting traffic primitives directly from naturalistically logged data for self-driving applications," *IEEE Robotics and Automation Letters*, vol. 3, no. 2, pp. 1223–1229, 2018.

[4] Y. Li, B. Li, X. Xu, and X. Sun, "A nonlinear decoupling control approach using RBFNNI-based robust pole placement for a permanent magnet in-wheel motor," *IEEE Access*, vol. 6, no. 1, pp. 1844–1854, 2018.

[5] Q. Song, H. Wan, Y. Mi, and S. Ye, "Optimum control strategy of drive torque for pure electric vehicles during acceleration," *Journal of Jiangsu University (Natural Science Edition)*, vol. 38, no. 1, pp. 1–6, 2017.

[6] R. Wang and J. Wang, "Actuator-redundancy-based fault diagnosis for four-wheel independently actuated electric vehicles," *IEEE Transactions on Intelligent Transportation Systems*, vol. 15, no. 1, pp. 239–249, 2014.

[7] W. Wang, H. Chen, Z. Diao, and J. Yang, "Investigation into automatic path tracking control System of autonomous electric vehicle based on photoelectric navigation," *Automotive Engineering*, vol. 30, no. 2, pp. 137–140, 2008.

[8] W. Wang, H. Chen, and Z. Diao, "A study on integrated chassis control for unmanned electric touring vehicle," *Automotive Engineering*, vol. 29, no. 8, pp. 681–686, 2007.

[9] B. Tan and W. Zhang, "Control of double-drive wheel motors in unmanned vehicles," *Journal of Xi'an Technological University*, vol. 31, no. 7, pp. 660–664, 2011.

[10] H. Her, Y. Koh, E. Joa, K. Yi, and K. Kim, "An integrated control of differential braking, front/rear traction, and active roll moment for limit handling performance," *IEEE Transactions on Vehicular Technology*, vol. 65, no. 6, pp. 4288–4300, 2016.

[11] J. L. F. Daya, P. Sanjeevikumar, F. Blaabjerg, P. W. Wheeler, and J. O. Ojo, "Implementation of wavelet-based robust differential control for electric vehicle application," *IEEE Transactions on Power Electronics*, vol. 30, no. 12, pp. 6510–6513, 2015.

[12] X. Yuan and J. Wang, "Torque distribution strategy for a front- and rear-wheel-driven electric vehicle," *IEEE Transactions on Vehicular Technology*, vol. 61, no. 8, pp. 3365–3374, 2012.

[13] L. Zhai, S. Dong, and K. Luo, "Electronic differential speed steering control for four in-wheel motors independent drive vehicle," in *2011 9th World Congress on Intelligent Control and Automation*, pp. 901–905, Taipei, Taiwan, June 2010.

[14] L. Jin, Q. Wang, X. Zhou, and C. Song, "Control strategy and simulation for electronic differential of vehicle with motorized wheels," *Journal of Jilin University (Engineering and Technology Edition)*, vol. 38, pp. 1–6, 2008.

[15] Z. Yu, J. Liu, L. Xiong, and Y. Feng, "Control strategies of handling improvement of distributed drive electric vehicle," *Journal of Tongji University (Natural Science)*, vol. 42, no. 7, pp. 1088–1095, 2014.

[16] J. Wang, Q. Wang, C. Song, L. Jin, and C. Hu, "Co-simulation and test of differential drive assist steering control system for four-wheel electric vehicle," *Transactions of The Chinese Society of Agricultural Machinery*, vol. 41, no. 6, pp. 7–14, 2010.

[17] C. Hu, R. Wang, F. Yan, and H. R. Karimi, "Robust composite nonlinear feedback path-following control for independently actuated autonomous vehicles with differential steering," *IEEE Transactions on Transportation Electrification*, vol. 2, no. 3, pp. 312–321, 2016.

[18] H. Jiang, C. Li, S. Ma, S. H. Ding, and C. Zhang, "Path tracking control of automatic parking for intelligent vehicle based on non-smooth control strategy," *Journal of Jiangsu University (Natural Science Edition)*, vol. 38, no. 5, pp. 497–502, 2017.

[19] C. Qian, X. Shen, Y. Zhang, Q. Yang, J. Shen, and H. Zhu, "Building and climbing based visual navigation framework for self-driving cars," *Mobile Networks and Applications*, vol. 23, no. 3, pp. 624–638, 2018.

[20] S. J. Anderson, S. B. Karumanchi, K. Iagnemma, and J. M. Walker, "The intelligent copilot: a constraint-based approach to shared-adaptive control of ground vehicles," *IEEE Intelligent Transportation Systems Magazine*, vol. 5, no. 2, pp. 45–54, 2013.

[21] T. H. Bryne, J. M. Hansen, R. H. Rogne, N. Sokolova, T. I. Fossen, and T. A. Johansen, "Nonlinear observers for integrated INS\/GNSS navigation: implementation aspects," *IEEE Control Systems Magazine*, vol. 37, no. 3, pp. 59–86, 2017.

[22] M. Khan, S. Hassan, S. I. Ahmed, and J. Iqbal, "Stereovision-based real-time obstacle detection scheme for unmanned ground vehicle with steering wheel drive mechanism," in *2017 International Conference on Communication, Computing and Digital Systems (C-CODE)*, pp. 380–385, Islamabad, Pakistan, March 2017.

[23] Y. Rasekhipour, A. Khajepour, S. K. Chen, and B. Litkouhi, "A potential field-based model predictive path-planning controller for autonomous road vehicles," *IEEE Transactions on Intelligent Transportation Systems*, vol. 18, no. 5, pp. 1255–1267, 2017.

[24] G. Yin, Z. Wang, and X. Jin, "Active steering of autonomous vehicle using model predictive control with Legendre function," in *2016 Chinese Control and Decision Conference (CCDC)*, pp. 3277–3281, Yinchuan, China, May 2016.

[25] W. Zhang, T. Mei, H. Liang et al., "Research and development of automatic driving system for intelligent vehicles," in *Foundations and Practical Applications of Cognitive Systems and Information Processing. Advances in Intelligent Systems and Computing, vol 215*, F. Sun, D. Hu, and H. Liu, Eds., pp. 675–684, Springer, Berlin, Heidelberg, 2014.

[26] J. Guo, P. Hu, L. Li, and R. Wang, "Design of automatic steering controller for trajectory tracking of unmanned vehicles using genetic algorithms," *IEEE Transactions on Vehicular Technology*, vol. 61, no. 7, pp. 2913–2924, 2012.

[27] M. Jalali, A. Khajepour, S. Chen, and B. Litkouhi, "Handling delays in yaw rate control of electric vehicles using model predictive control with experimental verification," *Journal of Dynamic Systems Measurement and Control*, vol. 139, no. 12, article 121001, 2017.

[28] B. Zhang, A. Khajepour, and A. Goodarzi, "Vehicle yaw stability control using active rear steering: development and experimental validation," *Proceedings of the Institution of Mechanical Engineers, Part K: Journal of Multi-body Dynamics*, vol. 231, no. 2, pp. 333–345, 2017.

[29] C. Hu, R. Wang, F. Yan, Y. Huang, H. Wang, and C. Wei, "Differential steering based yaw stabilization using ISMC for independently actuated electric vehicles," *IEEE Transactions on Intelligent Transportation Systems*, vol. 19, no. 2, pp. 627–638, 2018.

[30] E. Hashemi, M. Pirani, A. Khajepour, B. Fidan, A. Kasaiezadeh, and S. K. Chen, "Opinion dynamics-based vehicle velocity estimation and diagnosis," *IEEE Transactions on Intelligent Transportation Systems*, vol. 19, no. 7, pp. 2142–2148, 2018.

[31] J. Choi, K. Yi, J. Suh, and B. Ko, "Coordinated control of motor-driven power steering torque overlay and differential braking for emergency driving support," *IEEE Transactions on Vehicular Technology*, vol. 63, no. 2, pp. 566–579, 2014.

[32] Y. Huang, A. Khajepour, M. Khazraee, and M. Bahrami, "A comparative study of the energy-saving controllers for automotive air-conditioning/refrigeration systems," *Journal of Dynamic Systems, Measurement, and Control*, vol. 139, no. 1, article 014504, p. 9, 2017.

[33] X. Diao and H. Zhu, "Survey of decoupling control strategies for bearingless synchronous reluctance motor," *Journal of Jiangsu University (Natural Science Edition)*, vol. 38, no. 6, pp. 687–695, 2017.

[34] Y. Huang, A. Khajepour, T. Zhu, and H. Ding, "A supervisory energy-saving controller for a novel anti-idling system of service vehicles," *IEEE/ASME Transactions on Mechatronics*, vol. 22, no. 2, pp. 1037–1046, 2017.

[35] M. Li, S. Li, and B. Fan, "Research on solar collector simulation based on genetic-BP algorithm," *Proceedings of the Chinese Society of Electrical Engineering*, vol. 32, no. 5, pp. 126–130, 2012.

[36] Y. Liu, X. Zhu, and J. Yang, "Fault diagnosis of PV array based on optimised BP neural network by improved adaptive genetic algorithm," *The Journal of Engineering*, vol. 2017, no. 13, pp. 1427–1431, 2017.

[37] N. Zhang, C. Zhou, Z. Gao, and Y. Y. Li, "Torque distribution strategy of PHEV based on FCMAC neural network," *Journal of Jiangsu University (Natural Science Edition)*, vol. 38, no. 6, pp. 652–657, 2017.

[38] S. Liu, Z. Hou, and C. Yin, "Data-driven modeling for UGI gasification processes via an enhanced genetic BP neural network with link switches," *IEEE Transactions on Neural Networks and Learning Systems*, vol. 27, no. 12, pp. 2718–2729, 2016.

[39] J. Li, Q. Zhang, K. Wang, J. Wang, T. Zhou, and Y. Zhang, "Optimal dissolved gas ratios selected by genetic algorithm for power transformer fault diagnosis based on support vector machine," *IEEE Transactions on Dielectrics and Electrical Insulation*, vol. 23, no. 2, pp. 1198–1206, 2016.

[40] Y. Huang, H. Wang, A. Khajepour et al., "A review of power management strategies and component sizing methods for hybrid vehicles," *Renewable and Sustainable Energy Reviews*, vol. 96, pp. 132–144, 2018.

[41] Y. Yang, G. Wang, and Y. Yang, "Parameters optimization of polygonal fuzzy neural networks based on GA-BP hybrid algorithm," *International Journal of Machine Learning and Cybernetics*, vol. 5, no. 5, pp. 815–822, 2014.

[42] X. Xue, Y. Li, X. Yang, X. Chen, and J. Xiang, "Prediction of slope stability based on GA-BP hybrid algorithm," *Neural Network World*, vol. 25, no. 2, pp. 189–202, 2015.

[43] L. Zhuo, J. Zhang, P. Dong, Y. Zhao, and B. Peng, "An SA–GA–BP neural network-based color correction algorithm for TCM tongue images," *Neurocomputing*, vol. 134, pp. 111–116, 2014.

[44] D. Kasinathan, A. Kasaiezadeh, A. Wong, A. Khajepour, S. K. Chen, and B. Litkouhi, "An optimal torque vectoring control for vehicle applications via real-time constraints," *IEEE Transactions on Vehicular Technology*, vol. 65, no. 6, pp. 4368–4378, 2016.

[45] M. Jalali, S. Khosravani, A. Khajepour, S. K. Chen, and B. Litkouhi, "Model predictive control of vehicle stability using coordinated active steering and differential brakes," *Mechatronics*, vol. 48, pp. 30–41, 2017.

[46] M. Ataei, A. Khajepour, and S. Jeon, "A novel reconfigurable integrated vehicle stability control with omni actuation systems," *IEEE Transactions on Vehicular Technology*, vol. 67, no. 4, pp. 2945–2957, 2018.